AGU100 ADVANCING EARTH AND SPACE SCIENCE

Water Resources Research

RESEARCH ARTICLE
10.1029/2019WR025332

Key Points:
- A subsurface coupling length scale is established to estimate total column water changes from surface soil moisture observations
- The length scale is equivalent to the *e*-folding scale for soil profile covariance and the appropriate mass-conserving surface layer thickness for a bucket model
- Satellite-retrieved soil moisture provides information on more soil water than satellite radiometers can "see" for most of Earth's land surface

Supporting Information:
- Supporting Information S1

Correspondence to:
D. J. Short Gianotti,
gianotti@mit.edu

Citation:
Short Gianotti, D. J., Salvucci, G. D., Akbar, R., McColl, K. A., Cuenca, R., & Entekhabi, D. (2019). Landscape water storage and subsurface correlation from satellite surface soil moisture and precipitation observations. *Water Resources Research*, *55*, 9111–9132. https://doi.org/10.1029/2019WR025332

Received 9 APR 2019
Accepted 17 SEP 2019
Accepted article online 10 OCT 2019
Published online 16 NOV 2019

Landscape Water Storage and Subsurface Correlation From Satellite Surface Soil Moisture and Precipitation Observations

Daniel J. Short Gianotti[1], Guido D. Salvucci[2], Ruzbeh Akbar[1], Kaighin A. McColl[3,4], Richard Cuenca[5], and Dara Entekhabi[1]

[1]Parsons Laboratory, Massachusetts Institute of Technology, Cambridge, MA, USA, [2]Department of Earth and Environment, Boston University, Boston, MA, USA, [3]Department of Earth and Planetary Sciences, Harvard University, Cambridge, MA, USA, [4]John A. Paulson School of Engineering and Applied Sciences, Harvard University, Cambridge, MA, USA, [5]Department of Biological and Ecological Engineering, Oregon State University, Corvallis, OR, USA

Abstract Surface soil moisture measurements are typically correlated to some degree with changes in subsurface soil moisture. We calculate a hydrologic length scale, λ, which represents (1) the mean-state estimator of total column water changes from surface observations, (2) an *e*-folding length scale for subsurface soil moisture profile covariance fall-off, and (3) the best second-moment mass-conserving surface layer thickness for a simple bucket model, defined by the data streams of satellite soil moisture and precipitation retrievals. Calculations are simple, based on three variables: the autocorrelation and variance of surface soil moisture and the variance of the net flux into the column (precipitation minus estimated losses), which can be estimated directly from the soil moisture and precipitation time series. We develop a method to calculate the lag-one autocorrelation for irregularly observed time series and show global surface soil moisture autocorrelation. λ is driven in part by local hydroclimate conditions and is generally larger than the 50-mm nominal radiometric length scale for the soil moisture retrievals, suggesting broad subsurface correlation due to moisture drainage. In all but the most arid regions, radiometric soil moisture retrievals provide more information about ecosystem-relevant water fluxes than satellite radiometers can explicitly "see"; lower-frequency radiometers are expected to provide still more statistical information about subsurface water dynamics.

1. Introduction

Surface soil moisture—a small constituent of the land surface and the global water cycle—plays an outsized role in Earth system processes. It sits at the interface between the complex geological and atmospheric systems that comprise the terrestrial surface. Surface soil moisture couples the terrestrial water, energy, and carbon cycles (Green et al., 2019; Haghighi et al., 2018; Legates et al., 2011; Rigden et al., 2018; Short Gianotti et al., 2019); integrates the effects of weather to drive both water resource distribution and climate feedbacks (Jung et al., 2010; Koster et al., 2004; McColl et al., 2017; Taylor et al., 2012); drives the diffusive forces that support vegetative ecosystems (Barichivich et al., 2014; Muñoz et al., 2014; Van der Molen et al., 2011); constrains geomorphology, biogeography, and groundwater transfers (Legates et al., 2011); and serves as the bell-weather for drought and heatwaves (Bolten & Crow, 2012; Ciais et al., 2005; Hirschi et al., 2011; Miralles et al., 2014; Mueller & Seneviratne, 2012; Musyimi, 2011). For these reasons, a number of remote sensing projects have undertaken global measurement of the surface for soil moisture estimation, notably with the recent L-band microwave Soil Moisture Active Passive (SMAP; Entekhabi et al., 2010) and Soil Moisture and Ocean Salinity (Kerr et al., 2001) missions created specifically for this purpose. While these missions report measurements integrating radiometric emissions over a thin layer of the terrestrial surface, it is important to ask what, if anything, they can tell us about the hydrologic system beyond the upper few centimeters of the land surface.

The surface is only part of the story. The existence of root systems (down to tens of meters) attests to the water storage capacity of the soil subsurface. The deeper water volumes themselves are observable only through sparse in situ sensor networks, observation wells, or very coarse gravimetric estimates (e.g., GRACE mission; S. C. Swenson, 2012); otherwise, they are scientifically invisible. An ecosystem modeler

given satellite soil moisture retrievals may wonder if a specific drying event represents anything greater for the system as a whole.

There is a case to be made that the surface may tell us about the subsurface (Calvet & Noilhan, 2000; Entekhabi et al., 1994; Houser et al., 1998). Simple filtering of soil moisture time series from the upper few centimeters of the soil column is commonly an effective estimate of meter-scale subsurface state (C. Albergel et al., 2008; Ceballos et al., 2005) and can provide as much information for near-term vegetation dynamics and energy fluxes as integrated meter-scale soil moisture measurements (Qiu et al., 2014, 2016). This empirical evidence, along with a mature theory of flow in porous media, provides the scientific basis for root-zone soil moisture products from remotely sensed instruments (Ford et al., 2014; Reichle et al., 2017).

The distinction between surface and subsurface is a matter of utility. The remote sensing community often refers to "the surface" as whatever depth can be seen by a specific platform (typically tens of millimeters), while hydrologic modelers define discretized surface layer thicknesses (less than a millimeter to multiple meters or more) as appropriate for a given application. In this paper, we will think of the surface as a discrete soil layer whose moisture state we can characterize by observations (in situ or remotely sensed) and the subsurface as a region requiring inference, although we will use in situ measurements of the subsurface as well.

Process-based models suffer at coarse horizontal scale, where observations may not map explicitly onto model variables (consider a 9 km × 9 km × 5 cm uniform surface soil layer at the scale of satellite observations). Data assimilation approaches can ingest upscaled observations to circumvent this issue (Clément Albergel et al., 2019; Kumar et al., 2009, 2019; Ragab, 1995; Reichle et al., 2007, 2008; Sabater et al., 2007; Salvucci & Entekhabi, 2011), but some have argued that the theoretically fundamental relationships that govern soil moisture dynamics may not even be transferable across scales (Kirchner, 2009; e.g., does a watershed-scale soil integrated moisture observation follow Richards' equation?). In this study, we will draw on these ideas and focus on what data streams from the SMAP and Global Precipitation Measurement (GPM: Hou et al., 2014) missions tell us about subsurface soil moisture, and we will focus on a physical model which we expect to remain consistent at remote sensing scales, namely conservation of water mass.

The motivating question for this study is "What is the relationship between fluctuations in (satellite-observable) surface soil moisture and the larger pool of surface and subsurface water?" We will answer this in a first-order sense, and we will find that the answer is a length scale that represents the correlation between the surface and the greater soil moisture profile. We will refer to this length scale as the *subsurface correlation length*, λ. While we will define the scale through a simple regression equation which translates changes in surface soil moisture into changes in total column water, we will show that it is equivalent to (1) the *e*-folding scale for an exponential covariance profile and (2) the thickness of a uniform surface soil moisture layer for a bucket model which conserves water mass. Along the way, we will demonstrate a method for calculating the 1-day-lagged autocorrelation coefficient for time series data with missing observations and establish a variance budget for surface water balance.

1.1. Soil Moisture Length Scales

Remotely sensed observations integrate information over pixel areas as well as over some sensing or emission depth. For the microwave radiometric emissions used in passive soil moisture retrievals, the observed brightness temperature signal is a soil media-attenuated (and scattered/reflected/etc.) integral of the Earth's thermal emission. The vertical integration of the signal depends on a soil moisture and temperature-dependent attenuation function, with drier soils leading to deeper soil representation (Raju et al., 1995; Ulaby et al., 1986). Njoku and Entekhabi (1996) defined a commonly used representative emission depth as the distance in the soil medium over which the intensity of propagating radiation decreases by e^{-1} (at a given microwave frequency). While this and other effective radiometric emission depths are based on physical properties, any soil emission depth assigned to a particular soil moisture observation is inherently nonphysical (Zhou et al., 2016); every satellite radiometer retrieval is an unevenly weighted integration of emissions through the soil column and across heterogeneous areas, with the nearest depths contributing the most signal. To make use of these observations, an explicit scale is required; SMAP observations are assigned a nominal 50-mm depth (Entekhabi et al., 2014)—close to the range of *e*-folding penetration depths for the 1.41-GHz SMAP radiometer—with the idea that (1) retrieved soil moisture values are appropriate for a simple conceptual soil layer of 50 mm with uniform soil moisture throughout and (2) calibration and

validation between SMAP retrievals and point measurements or other remotely sensed products should use a corresponding depth for intercomparison.

The shallowness of this radiometric length scale has been at times criticized as a limitation for ecological and land-atmosphere interaction studies (C. Albergel et al., 2008; Li & Islam, 1999), and some have argued (using unlagged correlations between brightness temperatures and in situ soil moisture) that the nominal length should be closer to 20 mm for L-band radiometers (Escorihuela et al., 2010), or possibly less for very wet soils (Wang & Schmugge, 1980). In seeming contradiction, other studies have found that L-band surface soil moisture data seems to represent soil moisture processes deeper than the sensing depth (Qiu et al., 2014, 2016), that surface soil moisture encodes much of the water balance information observed in gravimetric water column retrievals (Crow et al., 2017), and that optimal model length scales for minimizing water budget errors are both generally larger than 50 mm and *increase* with wetter hydroclimatological conditions (Akbar et al., 2018a, 2019). This apparent contradiction, we argue, is due to greater physical and statistical correlation across the soil profile under wetter conditions (due to increased hydraulic conductivity), which is effectively independent of the notion of the radiometric depth.

2. Data

In this study, we use soil moisture data and precipitation data from two in situ sources—the United State Climate Reference Network (Bell et al., 2013) and seven carefully instrumented sites for the Airborne Microwave Observatory of Subcanopy and Subsurface (AirMOSS) campaign (Cuenca et al., 2016)—as well as from satellite retrievals from the SMAP mission (Entekhabi et al., 2010) and the GPM mission (Hou et al., 2014).

Our satellite soil moisture time series come from the SMAP Level 3 Passive Enhanced product (O'Neill et al., 2016)—a 6 AM local time snapshot—and our precipitation time series come from the gauge-corrected 30-min final run Level 3 GPM Integrated Multi-satellitE Retrievals for GPM product (Huffman et al., 2017), accumulated to daily 6 AM–6 AM local time totals. The precipitation data is regridded to the 9-km SMAP EASE-Grid 2 grid (Brodzik et al., 2012) using (WGS 84) area-weighted accumulations to conserve total water mass (all maps shown are equirectangular on the 9-km EASE-Grid 2 grid). The analysis window spans the overlapping window of the two data products—from SMAP's earliest available data (31 March 2015) through 30 June 2018.

Much of the analysis in this study relies on regressions of daily-scale soil moisture processes or time series variance estimates which can be strongly, spuriously influenced by both deterministic and stochastic low-frequency variability. The effects of stochastic drifts are removed by taking temporal first differences, and deterministic seasonality is removed through deseasoning. Prior to analysis, we remove the annual seasonal cycle from both the soil moisture and precipitation data at each location by (1) calculating the 365 daily average values of the variable in question over all observed years, (2) concatenating three copies of the 365-day annual climatology as a single time series to ensure exact periodicity, (3) smoothing the time series with a 61-day box filter (61 days chosen to minimize the effects of synoptic variability), and (4) subtracting the smoothed climatology from the original data to obtain anomaly series.

For SMAP soil moisture, any retrieval with more than 15% estimated surface water fraction or any frozen soil or snow cover surface quality flags is removed from the analysis. Vegetation water content (VWC) can impact microwave soil moisture retrieval quality, and seasonal maps of SMAP VWC greater than 5 kg/m^2 are shown in Figure S1 in the supporting information.

3. Derivation of the Subsurface Coupling Length Scale

Consider a one-dimensional soil column with volumetric soil moisture profile $\theta(z)$—the surface is at $z = 0$ and z increases positively with depth. The total soil moisture in this column is given by

$$V = \int \theta(z)\, dz, \tag{1}$$

with units of length, and this volume changes in time under the influences of infiltration, surface evaporation, root system transport for transpiration, and deep drainage (depending on vertical extent of the

integral). We will ignore the effects of horizontal moisture advection for grids with large (>80 km^2) areas throughout this study.

While we may be interested in these changes in total column storage, our vision of Earth's water is typically limited by surface instrumentation or remotely sensed estimates of surface states. Given a data stream of surface soil moisture estimates (whether in situ or remotely sensed), $\theta_s(t)$, we might try to estimate changes in V using changes in θ_s. This can be done using Richards' equation and any number of data assimilation schemes, although issues of heterogeneity and sensitivity to nonlinear process can sometimes swamp the information provided by boundary conditions. We may also be interested in the correlation structure of the vertical soil moisture profile and how it varies across sites. To the extent that the surface is correlated with the subsurface (through diffusion and gradient-induced fluxes, root-driven surface/subsurface coupling, auto-correlation of precipitation, etc.), we can propose a simple linear model as follows:

$$\frac{dV}{dt} = \lambda \frac{d\theta_s}{dt} + \varepsilon_{reg}(t), \tag{2}$$

where λ is some scaling parameter (with units of length) and ε_{reg} is a mean-zero error (unexplained variance) term accounting for the error in assuming a linear, static model relating the surface and subsurface (the errors are not assumed to be Gaussian and are almost certainly not in practice as evident from mixing wetting and drying processes). This is a simple regression equation, and we can write the least-squares estimator of λ as a ratio of covariances and variances as follows:

$$\lambda = \frac{\langle V', \theta_s' \rangle}{\sigma^2_{\theta_s'}} \tag{3a}$$

$$= \frac{\sigma_{V'} \cdot \rho(V', \theta_s')}{\sigma_{\theta_s'}} \tag{3b}$$

$$= \sqrt{\frac{\sigma^2_{V'} - \sigma^2_{\varepsilon_{reg}}}{\sigma^2_{\theta_s'}}}, \tag{3c}$$

with $\langle \cdot \rangle$ brackets indicating covariances, σ^2 indicating variances, $\rho(\cdot)$ indicating correlation, and prime ($\dot{\theta}$) superscripts indicating time derivatives. It is worth noting that the least-squares estimate assumes exogeneity (no correlation between $d\theta_s/dt$ and ε_{reg}), which may introduce estimation errors in-situations with extreme matric potential gradients, such as those driving capillary rise, particularly for small scale (e.g., in situ) measurements.

Since λ scales the surface observations to represent changes in volume beyond the surface, we will refer to it as the "subsurface coupling length" associated with a given surface layer thickness.

3.1. A Two-Layer Model

Figure 1 shows a simple representation of the soil column. The surface layer has thickness h_1, defined by the characteristics of in situ sensors or the radiometric sensing depth of a satellite-based sensor. The (depth-averaged) volumetric soil moisture in the surface layer is given by

$$\theta_s = \frac{1}{h_1} \int_0^{h_1} \theta(z)\, dz, \tag{4}$$

and we assume that observations (from in situ or satellite-based sensors) are representative of this value. In the case of remotely sensed radiometric observations, h_1 is the radiometric sensing depth.

The subsurface consists of the soils below $z = h_1$, which we allow to extend to some arbitrary, large static thickness h_2. At the lower extents of the subsurface layer, we might expect volumetric soil moisture to be more slowly variable than at the surface and perhaps totally uncorrelated with surface observations. We do not assume constant soil moisture with depth in the subsurface, nor constant correlation with the

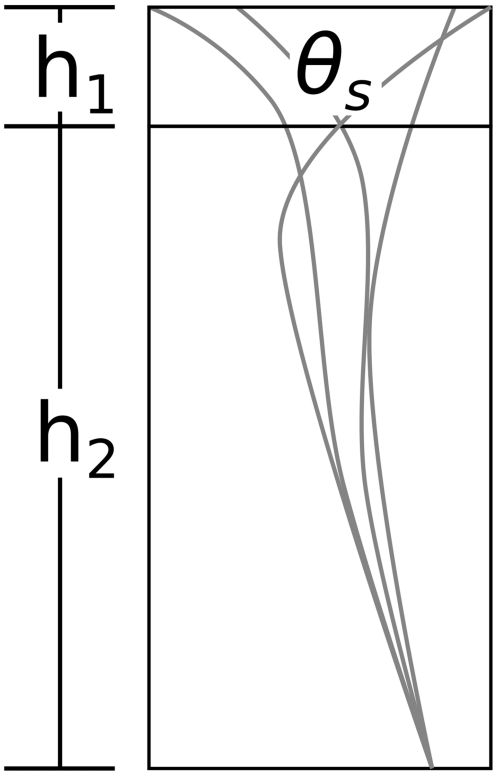

Figure 1. A one-dimensional soil column model. The (observed) surface layer is defined by thickness h_1 and mean volumetric soil moisture is given by $\theta_s = \frac{1}{h_1} \cdot \int_0^{h_1} \theta(z)\, dz$. The subsurface is represented by a column extending to an arbitrary, large depth h_1+h_2, with variable soil moisture profile.

surface layer with depth. The mean subsurface volumetric soil moisture at any time (without assuming that soil moisture behaves as its mean value) is given by

$$\theta_{sub}(t) = \frac{1}{h_2} \int_{h_1}^{h_1+h_2} \theta(z,t)\, dz. \tag{5}$$

We can write the changes in total column storage as

$$\frac{dV}{dt} = h_1 \cdot \theta_s' + h_2 \cdot \theta_{sub}', \tag{6}$$

and write equations (3a) and (3b) as

$$\lambda = \frac{h_1 \cdot \theta_s' + h_2 \cdot \theta_{sub}', \theta_s'}{\sigma^2_{\theta_s'}} \tag{7a}$$

$$= h_1 + h_2 \cdot \frac{\sigma_{\theta_{sub}'} \cdot \rho(\theta_s', \theta_{sub}')}{\sigma_{\theta_s'}}, \tag{7b}$$

which shows that λ is greater than h_1 and less than h_1+h_2 whenever the surface and subsurface layers positively covary. Additionally, when θ_s' and θ_{sub}' are uncorrelated, the lower bound $\lambda = h_1$ applies, and our best statistical estimate for dV is $\lambda \cdot d\theta_s = h_1 \cdot d\theta_s$.

Equations (7a) and (7b) are exact in terms of representing λ in equations (3a) and (3b) and do not rely on any assumptions about truly linear relationships between soil layers or on Gaussian errors. However, they are of

Table 1
Site Characteristics for in Situ AirMOSS Sites

Site	Observation period	Mean annual precipitation (cm)	Total observed column depth (cm)	λ (cm; $h_1 = 3.5$ cm)
Chamela, JA (MX)	2013–2015	67.2	57.5	18.0
Duke Forest, NC (USA)	2011–2015	69.1	80	25.0
Harvard Forest, MA (USA)	2011–2015	90.0	80	22.8
Metolius, OR (USA)	2011–2015	71.9	90	19.2
BERMS Old Aspen, SK (CA)	2013–2015	11.8	90	28.1
BERMS Old Jack Pine, SK (CA)	2012–2015	37.5	90	20.5
Tonzi Ranch, CA (USA)	2012–2015	49.5	90	13.5

limited utility in estimating a length scale or anything about surface-subsurface correlation as they depend on (1) second-order subsurface statistics (which are typically unobserved), (2) the surface-subsurface correlation itself, and (3) h_2, which we have only defined thus far as arbitrary and large.

We can, however, explore the relationships in equations (7a) and (7b) at sites with available soil moisture profile measurements. Table 1 shows characteristics for seven in situ sites with sensors at multiple depths and replicate sensor profiles installed for the AirMOSS P-band soil moisture investigation (Tabatabaeenejad et al., 2015). These are high-quality calibration sites, with shallow sensors at 2 cm down to multiple tens of centimeters. The subsurface coupling lengths λ using the uppermost sensor ($h_1 = 3.5$ cm) as "surface observations" are shown in the last column of Table 1 calculated using equation (7a) and soil moisture measurements.

Moisture profiles are estimated as M layers of uniform soil moisture around the M sensors at a given site, with uniform soil moisture within the layers (rather than interpolated). h_1 can be defined, then, using the uppermost sensor (as in Table 1), or a depth-weighted average of the two uppermost sensors, and so forth.

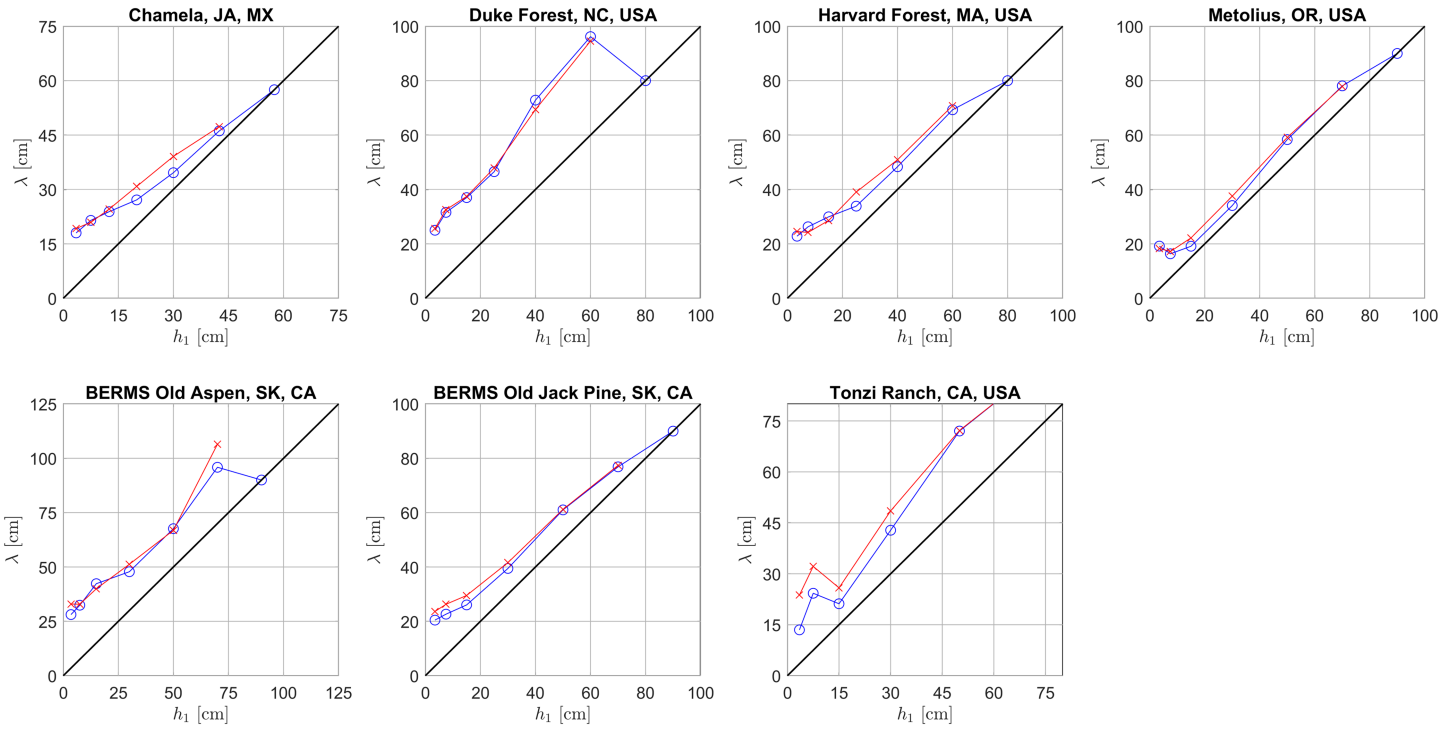

Figure 2. Regression coefficients, λ, versus the surface layer depth, h_1, at seven in situ sites (June–August). Blue circles show λ estimated directly from regression of the change in measured root zone soil moisture against changes in surface soil moisture to depth h_1, following equation (2). Red x-es show $\widehat{\lambda}$ as estimated from equation (A2), assuming an exponential correlation length. Correlation lengths (on the order of tens of centimeters) are shown in Figure S2.

Figure 2 shows λ as a function of h_1, the surface layer thickness, again using equation (7a) and soil moisture measurements. Daily snapshots of soil moisture from 3–5 years from 2011–2015 are deseasoned prior to regression, although the effect of deseasoning is minimal on λ using equation (2) directly. The blue circles in each subplot show λ calculated by regressing changes in total column storage (to a depth h_1+h_2 between 50 and 90 cm, depending on the deepest sensor at each site) on changes in the surface soil moisture for different surface layer thicknesses, h_1.

3.2. Dependence on Surface Layer Thickness

The subsurface coupling length, λ, generally increases with increased surface layer thickness, as seen in the positive slopes of the blue lines in Figure 2; the exception around $h_1 = 10$ cm at Tonzi Ranch is due to anticorrelation between two layers/sensors in the shallow subsurface. λ is also above the one-to-one ($\lambda = h_1$; no correlation between surface and subsurface) line, which demonstrates that the profile is statistically coupled in the z-direction. The fact that $\lambda > h_1$ tells us that the surface has predictive power for the subsurface, and the distance $\lambda - h_1$ tells us how much additional information the surface contains about the soil column below.

When h_1 reaches the depth of the deepest measured soil layer, the surface is a perfect predictor of the total column water to that depth, and so $\lambda = h_1$. At Chamela and Tonzi Ranch, λ reaches the depth of the deepest sensor before h_1, which suggests that the last 15–20 cm are static in volumetric water content. At the other extreme, the overshoot at the BERMS Old Aspen site suggests that there may be substantially more active, correlated soil moisture below a meter which we are unable to regress against due to the limit of the sensor depth.

4. Covariance *e*-Folding Equivalency

A common simplified soil moisture model for an unobserved subsurface profile is that the covariance or correlation falls off exponentially with depth, which we explore here. If rather than the proposed model of $V^{'}$ in equation (2), we instead linearly model changes in volumetric soil moisture at a depth z using the surface, then

$$\theta^{'}(z,t) = \gamma(z)\cdot\theta_s^{'}(t) + \omega(z,t) \tag{8}$$

As in equation (3),

$$\gamma(z) = \frac{\theta_s^{'},\theta_z^{'}}{\sigma^2_{\theta_s^{'}}} \tag{9a}$$

$$= \frac{\sigma_{\theta_z^{'}}\cdot\rho\left(\theta_s^{'},\theta_z^{'}\right)}{\sigma_{\theta_s^{'}}}, \tag{9b}$$

where $\theta_z^{'}$ is used for convenience in place of $\theta^{'}(z,t)$.

If we assume that the covariance between the surface layer and any arbitrary subsurface layer falls off exponentially,

$$\theta_s^{'},\theta_z^{'} = \sigma^2_{\theta_s^{'}}\cdot\exp\left(-\frac{z}{\kappa}\right), \tag{10}$$

then

$$V^{'} = \int_0^{h_1+h_2} \theta^{'}(z,t)\,dz \tag{11}$$

$$= \int_0^{h_1+h_2} \gamma(z)\cdot\theta_s^{'}(t) + \omega(z,t)\,dz \tag{12}$$

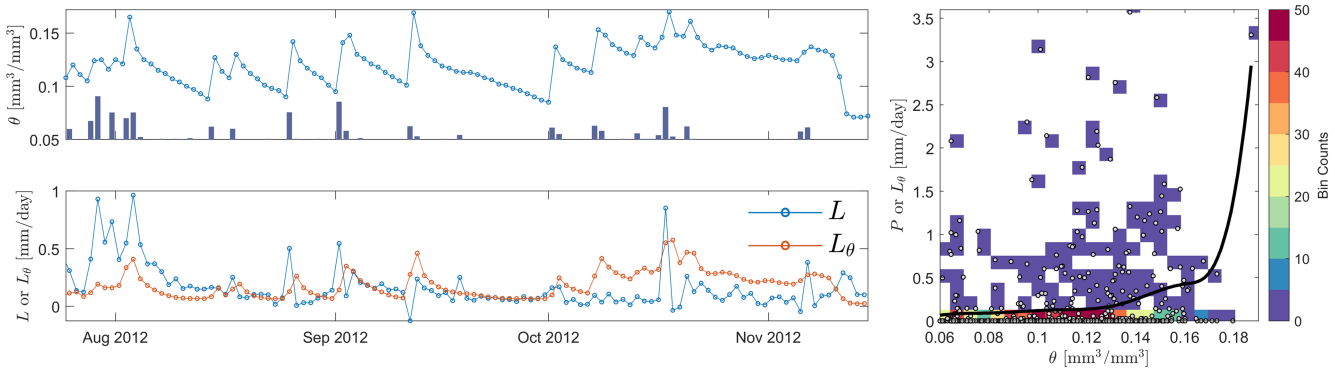

Figure 3. Time series of soil moisture, precipitation, and losses at BERMS Old Jack Pine in autumn 2012. The upper panel shows daily in situ volumetric soil moisture in light blue dots and precipitation in dark blue bars. The lower panel shows daily total profile losses in light blue and estimated total profile losses, L_θ, in red. L_θ is estimated as a function of soil moisture as in equation (21), as shown in the right panel. Gray dots in the right panel are coincident precipitation/soil moisture pairs, background coloring is a 2-D histogram of observation density, and the black line is the estimated function form of L_Θ calculated as the conditional average precipitation for a given soil moisture value.

$$= \int_0^{h_1+h_2} \frac{\theta_s', \theta_z'}{\sigma^2_{\theta_s'}} \cdot \theta_s'(t) + \omega(z,t)\, dz \tag{13}$$

$$= \int_0^{h_1+h_2} \exp\left(-\frac{z}{\kappa}\right) \cdot \theta_s'(t)\, dz + \int_0^{h_1+h_2} \omega(z,t)\, dz \tag{14}$$

$$= -\kappa \cdot \theta_s'(t) \cdot \left[\exp\left(-\frac{h_1+h_2}{\kappa}\right) - 1\right] + \Omega(t), \tag{15}$$

where $\Omega(t)$ is the integrated error term. For a true asymptotic exponential covariance profile, we let covariance approach zero with depth by letting $h_2 \to \infty$ and find that

$$V' = \kappa \cdot \theta_s' + \Omega(t), \tag{16}$$

which is exactly equation (2) with a different notation. In fact, least-squares constraints on equations (2) and (8) require that $\Omega(t) = \varepsilon(t)$ and $\kappa = \lambda$, which mean that the subsurface coupling length λ is also the covariance e-folding depth linking the surface and subsurface.

Appendix A contains further details of exponential covariance and correlation functions in the subsurface as well as bounds on the correlation length scale ($h_1 \leq \lambda \leq \sigma_{V'}/\sigma_{\theta_s'} \leq 2\sigma_P/\sigma_{\theta_s'}$). Global maps of the upper bounds are shown in Figure S9.

5. Approximating λ with only Surface Soil Moisture and Precipitation

Until this point, we have used in situ soil moisture at multiple depths in the column to determine surface/subsurface coupling length scales. While useful as a summary statistic or site characteristic, λ is of limited application use when full information about the subsurface is already known. In most locations, we do not have measurements of subsurface dynamics, although global surface soil moisture time series are available as retrievals from radiometric remote sensing platforms such as SMAP (Entekhabi et al., 2010), Soil Moisture and Ocean Salinity (Kerr et al., 2010), Advanced Scatterometer (Bartalis et al., 2007), and Advanced Microwave Scanning Radiometer (Imaoka et al., 2012; Kawanishi et al., 2003). Estimation of λ at sites without subsurface observations would (1) allow us to estimate first-order changes in landscape water storage behavior from these remotely sensed time series globally and (2) demonstrate the degree to which surface observations represent landscape-level changes more applicable to ecosystem analysis and drought definitions.

We can write the water balance (conservation of mass) equation as

$$\frac{\mathrm{dV}}{\mathrm{dt}} = \mathrm{P(t)} - \mathrm{L(t)}, \tag{17}$$

where $P(t)$ is the precipitation rate and $L(t)$ is an unobserved loss function incorporating soil evaporation, root uptake for transpiration, vertical drainage, interception losses, horizontal advection, and surface runoff. Although we hypothesize that at the scale of microwave satellite retrievals, (1) horizontal advection is minimal compared to vertical fluxes and (2) surface runoff is almost entirely reinfiltrated within the pixel, these assumptions are not necessary for our applications of equation (17).

5.1. A Variance Budget

Using our mean state estimator of dV/dt, we can write a variance budget form of the water balance equation as follows:

$$\mathrm{var}\left\{\lambda \cdot \theta_s^{'}\right\} = \mathrm{var}\{P_t - L_t\}, \tag{18}$$

and solve for λ as

$$\lambda = \frac{\sigma^2_{\mathrm{P-L}}}{\sigma^2_{\theta_s^{'}}}, \tag{19}$$

from which we will determine subsurface coupling lengths globally from satellite data. While (gauge-corrected) precipitation (P) data are available from the GPM satellite, outflow losses (L) from the surface layer are not and will need to be estimated. Additionally, while surface soil moisture time series θ_s are available, their daily derivative is not from the SMAP satellite directly (as overpass intervals vary from 1–3 days), and so care will be needed to calculate $\sigma^2_{\theta_s^{'}}$ as well.

5.2. Estimated Subsurface Losses

Salvucci (2001) offers an estimate of soil moisture losses from stationary surface soil moisture time series based on the derived theorem that the expected value $E\left\{\theta_s^{'} | \theta_s\right\} = 0$; that is, conditioned on any soil moisture state, changes in soil moisture are mean zero (upcrossings of θ_s must be balanced by downcrossings). This holds true at any time scale with sufficient observations to estimate the expectation. The first moment loss function conditioned on soil moisture state can then be written as

$$\begin{aligned} \mathrm{E}\left\{\theta_s^{'} | \theta_s\right\} &= \mathrm{E}\{\mathrm{P} - \mathrm{L} | \theta_s\} \\ &= \mathrm{E}\{\mathrm{P} | \theta_s\} - \mathrm{E}\{\mathrm{L} | \theta_s\} \\ &= 0 \end{aligned} \tag{20}$$

so that

$$\mathrm{E}\{\mathrm{L} | \theta_s\} = \mathrm{E}\{\mathrm{P} | \theta_s\}. \tag{21}$$

This relation provides a means of producing time series estimates of daily soil moisture losses from observed surface soil moisture and precipitation time series (see Figure 3), and we will denote this estimated loss as L_θ.

To estimate L_θ from equation (21), we fit a spline function to observed precipitation versus soil moisture pairs as shown in Figure 3. We use a spline toolbox (the Shape Language Modeling Toolbox in MATLAB) with six "knots" (spline breakpoints) and an increasing monotonicity constraint (L_θ increases with increasing soil moisture due to increasing hydraulic conductivity). To meet the stationarity constraints of the conditional averaging method, accumulated precipitation between soil moisture observations is paired with mean soil moisture from the two observations. $L_\theta(t)$ is determined by then evaluating the value of the fit spline function at the midpoint between soil moisture observations so that one loss value is calculated for each window between observations.

See Appendix A for full validation of loss function terms.

5.3. The Denominator of Equation (19)

The denominators—$\sigma^2_{\theta_s'}$—of equations (3), (9a), and (19) are calculated from snapshot observations of soil moisture (either from in situ sensors or remotely sensed retrievals). For in situ networks, these observations are available daily, and the variance terms are easily calculated by (1) taking a time series of (midnight) soil moisture snapshots, (2) calculating daily differences, and (3) taking the variance of the resulting difference time series. For remotely sensed observations, soil moisture may not be available daily and overpasses may not be spaced at regular time intervals. For the SMAP mission, retrievals are at 6 AM local time, and subsequent overpasses are 1–3 days apart, varying in an exact repeating 8-day pattern at each location. Since back-to-back observations are rare, a more robust method for estimating $\sigma^2_{\theta_s'}$ is desired.

For an arbitrary time-step Δt, note that

$$\mathrm{var}\left\{\frac{\Delta\theta_s}{\Delta t}\right\} = \frac{1}{(\Delta t)^2}\mathrm{var}\{\theta_s(t) - \theta_s(t-\Delta t)\}$$

$$= \frac{1}{(\Delta t)^2}[\mathrm{var}\{\theta_s(t)\} + \mathrm{var}\{\theta_s(t-\Delta t)\} - 2\,\theta_s(t), \theta_s(t-\Delta t)]. \quad (22)$$

For a stationary soil moisture process, the variances of $\theta_s(t)$ and $\theta_s(t - \Delta t)$ are identical and the covariance (by definition) is just that variance times the lag-1 autocorrelation (AR(1)) coefficient, ϕ, as follows:

$$\mathrm{var}\left\{\frac{\Delta\theta_s}{\Delta t}\right\} = \frac{1}{(\Delta t)^2}[2\,\mathrm{var}\{\theta_s\} - 2\,\phi\cdot\mathrm{var}\{\theta_s\}]$$

$$= \frac{2(1-\phi)}{(\Delta t)^2}\,\mathrm{var}\{\theta_s\}. \quad (23)$$

For a daily time-scale, $\Delta t = 1$ day and

$$\sigma^2_{\theta_s'} = 2(1-\phi)\cdot\sigma^2_{\theta_s}. \quad (24)$$

Despite involving an AR(1) coefficient, equation (24) is exact and does not require soil moisture to be well represented by an AR(1) model. In contrast to the variance of surface soil moisture differences, the variance of the surface soil moisture itself on the right-hand side of equation (24) is easily calculated from irregularly sampled time series (simply the variance of all observations). For the stationarity assumption to hold, soil moisture time series must be deseasoned prior to analysis.

5.3.1. Estimating the AR(1) Coefficient From Irregularly Spaced Observations

One method to calculate ϕ from a time series with missing data is to use a Kalman filter with no observation error term and AR(1) latent variable model. As a more analytical alternative, if the largest gap between daily observations is, say, 3 days, one can estimate ϕ as the positive root of

$$n_1\phi + n_2\phi^2 + n_3\phi^3 = \frac{n_1 v_1 + n_2 v_2 + n_3 v_3}{v_0}, \quad (25)$$

where n_1 is the number of pairs of 1-day-lagged observations, n_2 is the number of 2-day-lagged observations, n_3 is the number of 3-day-lagged observations, v_0 is the variance of all nonmissing observations, v_1 is the covariance between all 1-day-lagged pairs ($\langle\theta_t, \theta_{t+1}\rangle$ for all nonmissing observations on days t, t+1), v_2 is the covariance between all 2-day-lagged pairs, and v_3 is the covariance between all 3-day-lagged pairs. This can be expressed more generally as

$$\sum_i n_i \phi^i = \frac{1}{v_0} \sum_i n_i v_i \tag{26}$$

for data sets with gaps longer than 3 days. With no missing data, equation (26) collapses to the common least-squares estimator for the AR(1) coefficient as follows:

$$\hat{\phi} = \frac{\theta_t, \theta_{t+1}}{\sigma_\theta^2}. \tag{27}$$

These analytical estimates require sufficient data length for proper estimates. In this study, for computational efficiency, we use the analytical estimates whenever equation (25) has a single root $0 < \phi < 1$, and the Kalman filter otherwise (differences in estimates are negligible when both are feasible).

Global maps of the 9-km AR(1) coefficient, ϕ, for SMAP surface soil moisture are shown in Figure 4a. Even after deseasoning (which removes much of the integrated nature of the nonstationary storage processes), autocorrelation is high globally, typically above 0.5 and often above 0.9 (patterns in Figure 4 look similar with not-deseasoned soil moisture, with somewhat higher ϕ values). Soil moisture (and particularly surface soil moisture) is *not* expected to be well modeled by a simple autoregressive model with Gaussian errors at daily time scales due to the very non-Gaussian effect of precipitation forcing (although it does become more like an AR(1) process as the spatial scale increases). The magnitude of ϕ, nonetheless, tells us about the persistence of θ_s over time, either through the variability of rainfall or through the magnitude of surface soil moisture response to variable rainfall events (e.g., we would expect well-drained, coarse soils to have low autocorrelation, particularly in areas with irregular, intense storms). Contrast the strongly intermittent hydroclimate of the Sahel with the neighboring tropical Sudanian Savanna.

Beyond this, we would expect the inherent noise in soil moisture retrievals (0.04 mm^3/mm^3 or less for SMAP, as per mission requirements) to lead to lower values of ϕ in arid areas with lower signal-to-noise ratios. This appears possible in Figure 4a as well, with low values in the Sahara and Gobi deserts. Stochastic simulations (see Figure S3) suggest that while retrievals of ϕ are less accurate when ϕ is lower, errors in ϕ estimation are almost always less than 10% or less of the true value, and usually less than 5%.

Figure 4b shows the same ϕ values over the Contiguous United States (ConUS), with overlain ϕ values from the 81 United State Climate Reference Network stations. We argue that these are well-estimated values for both remotely sensed and in situ observations and that differences are due to spatial representation rather than estimation method. While we would not expect ϕ to match across spatial aggregation scales (and spatial correlations between ϕ_{USCRN} and ϕ_{SMAP} are low, ~0.3), the in situ and remotely sensed surface AR(1) coefficients are close in magnitude (RMSE ~0.1). In situ ϕ values are generally higher, which helps explain the larger in situ λ values shown in Figure A2c. Figure 4c shows the joint distribution of ϕ and mean surface soil moisture, which are positively correlated across climate conditions, at least up to a mean θ_s value of 0.25 cm^3/cm^3. The lag-one autocorrelation is estimated separately by season in Figure S4.

6. Global λ from Satellite Retrievals

Combining equations (19) and (24) gives us the ability to estimate the subsurface coupling length (estimates denoted as $\hat{\lambda}$) from irregularly observed remotely sensed data as follows:

$$\hat{\lambda} = \frac{\sigma_{P-L_\theta}}{\sigma_{\theta_s} \cdot \sqrt{2(1-\phi)}}. \tag{28}$$

Equation (28) suggests that $\hat{\lambda}$ increases with the variance of $P - L$, the net inflow to the system, and decreases with increasing var$\{\theta_s\}$. This makes intuitive sense; a large $\hat{\lambda}$ corresponds to large correlations with the subsurface which serve to buffer θ_s from large infiltration shocks. Equivalently, if θ_s changes substantially with small precipitation inputs, it is unlikely to represent correlated storage changes across the profile. The standard deviation ratio $\sigma_{P-L}/\sigma_{\theta_s}$ can be thought of as an "inertia to shocks," and is discussed in greater detail in Figure S5.

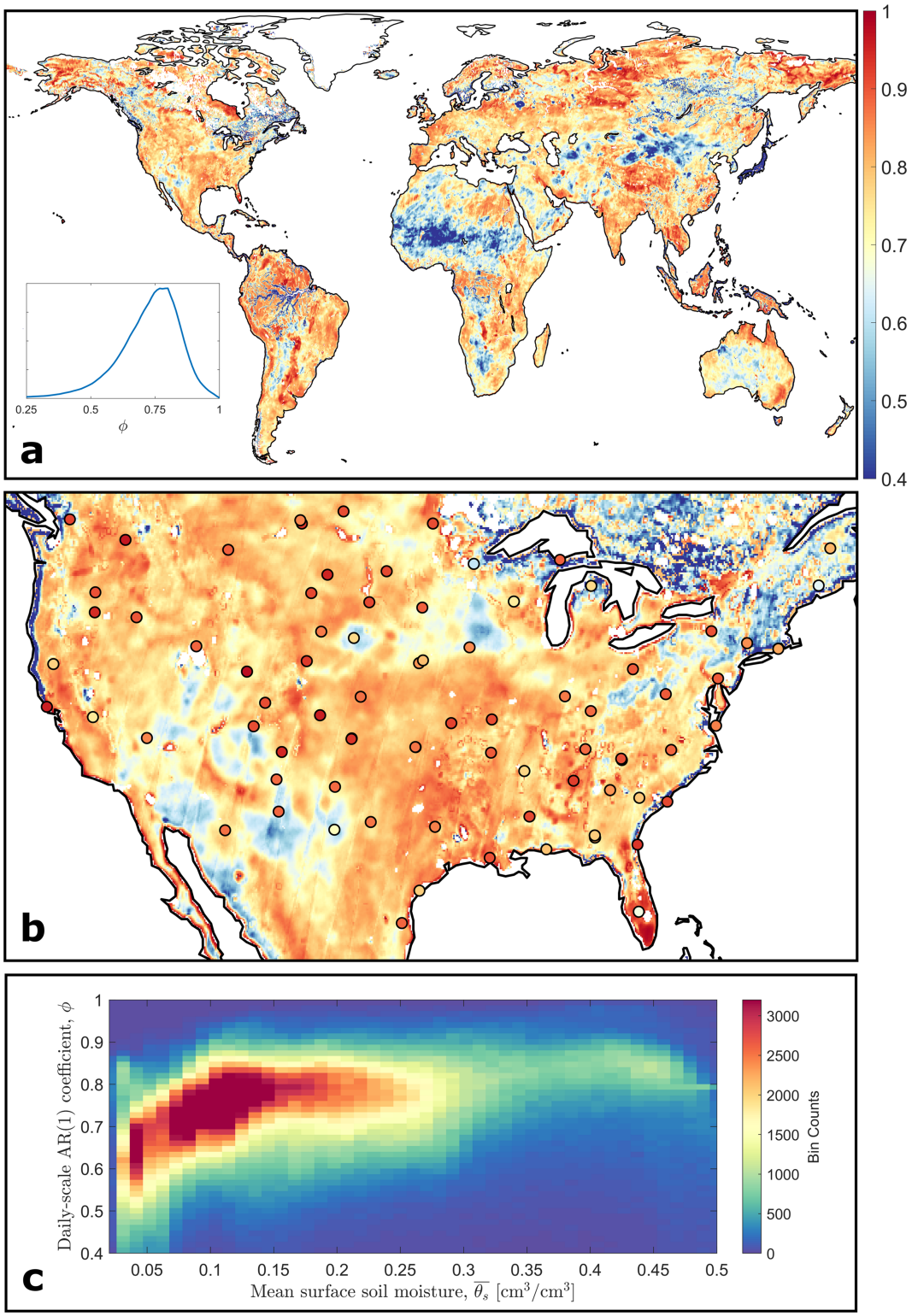

Figure 4. Daily-scale lag-one autocorrelation, ϕ, for deseasoned surface soil moisture. (a) ϕ from 9 km Soil Moisture Active Passive (SMAP) surface soil moisture. (b) Background same as (a) over ConUS; the markers show ϕ from in situ United State Climate Reference Network sites using surface layer $h_1 = 7.5$ cm. (c) Joint distribution of pixel-by-pixel ϕ and mean SMAP surface soil moisture showing positive correlation across arid/semiarid climate conditions. ConUS = Contiguous United States.

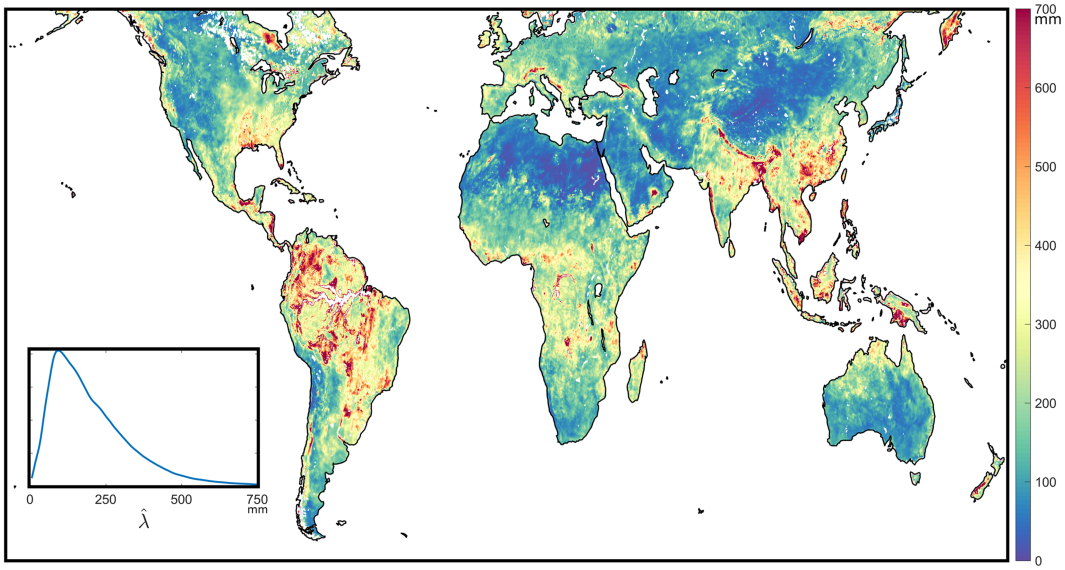

Figure 5. Estimated subsurface coupling length $\hat{\lambda}$, as calculated from equation (28) using Soil Moisture Active Passive surface soil moisture and Global Precipitation Measurement precipitation.

Combining these standard deviation ratios with the autocorrelation term $1/\sqrt{2(1-\phi)}$ gives us $\hat{\lambda}$, as shown in Figure 5. The subsurface coupling length scale is nearly always larger than the nominal sensing depth of SMAP (50 mm) and exceeds half a meter in many locations, particularly wet regions (Southeastern ConUS, Northern South America, Central Africa, Southeast Asia, and the Malay Archipelago). Mountainous regions with large $\hat{\lambda}$ values—notably the Alps, Caucasus, and Southwestern Himalayas—display both large precipitation variability (due in part to orography-driven high mean precipitation rates) and small soil moisture variability. In these regions, the impacts of lateral hillslope runoff may lead to larger differences between precipitation and infiltration, which could lead to overestimation of the numerator of equation (28).

The general spatial patterns in Figure 5 match the map of column water capacity obtained from a model (Figure 1 in Koster & Suarez, 2001), with larger subsurface coupling length scales in wet areas. The ConUS region during the summertime shows a high degree of similarity to estimates of a related length scale in Akbar et al. (2018b) made using explicit time series models rather than a variance budget. As we might expect, $\hat{\lambda}$ is strongly (positively) correlated with mean precipitation, mean soil moisture, ϕ, and an independent evapotranspiration data set (Moderate Resolution Imaging Spectroradiometer; Mu et al., 2013, see Figure S6).

It is worth noting that geographical differences between hydrologic length scales are *not* reflecting differences in radiometric sensing depth/emission depth. This is apparent because—unlike the radiometric sensing depth—the hydrologic length scale *increases* empirically with mean soil moisture (again, see Figure S6). This demonstrates that regardless of how the radiometric sensing depth is defined (whether static as 50 mm or as a dynamic function of soil moisture), the scaling factor $\hat{\lambda}$ is responding to fundamentally different processes, namely coupling of moisture fluxes between the surface layer that is "seen" by the SMAP radiometer and the deeper subsurface soil moisture.

The probability density function of $\hat{\lambda}$ across space (Figure 5, inset) does have a mode somewhat above the nominal 50-mm depth for the SMAP radiometer, suggesting many (arid) areas with minimal subsurface coupling. Global mean values range from 185–200 mm seasonally (see Figure S7).

7. Discussion

Regions with large subsurface coupling lengths (Figure 5) are typically wet (implying typically larger hydraulic conductivities; Figure S6) and display a high surface soil moisture autocorrelation (ϕ; Figure 4).

We would intuitively think that in these regions—where fluxes of water are large, but changes in the surface moisture state are small (Figure S5)—the landscape acts like a larger, more uniform "bucket," and indeed we find that the correlations between the surface and the subsurface are high. The surface encodes more information about the subsurface in these areas, and the first-order changes in surface soil moisture represent more movement of landscape water—volumes quantified by $\lambda \cdot \theta_s'$ instead just the observed $h_1 \cdot \theta_s'$. This implies greater utility for landscape or ecological applications.

Previous studies have estimated length scales from L-band soil moisture and precipitation data using a water balance framework (Akbar et al., 2018a; Crow et al., 2017). We suggest that these relationships are both statistical and physical, with drainage fluxes providing the coupling link between the surface and the soil profile as a whole. Greater drainage can lead to larger stores of column water, which seems to imply higher water-holding capacities which are typically larger in wet areas with high moisture persistence/autocorrelation (Koster & Suarez, 2001). Areas with large λ values are of particular importance for vegetative ecosystem modeling due to the link between precipitation storage capacity and root zone development (Milly, 1993, 1997), and larger surface soil moisture reservoir sizes lead to decreased runoff, increased evapotranspiration, and changes in offshore advective water transport with a positive feedback through vapor pressure deficit (Milly & Dunne, 1994).

The variance budget approach described in section 5 yields almost identical results to what can be obtained by expressing the water budget directly in terms of an active, but unobservable (i.e., "latent state variable") storage volume (i.e., $dV/dt = \text{Inputs} - \text{Outputs}$). This latent variable model can be combined with a measurement equation (i.e., $V = \lambda \cdot \theta$) in a state-space framework, and a Kalman filter can be used to infer the value of λ as an unknown coefficient. Our variance budget method, however, is simpler and yields an explicit equation for $\widehat{\lambda}$ with similar results (not shown).

The fact that λ is generally larger than SMAP's nominal radiative sensing depth of 50 mm, it shows that there is often substantial subsurface correlation, which explains previous findings that surface soil moisture retrievals demonstrate more explanatory power than might be physically expected (Crow et al., 2017; Qiu et al., 2014, 2016). Surface soil moisture appears to represent processes deeper into the root zone than radiometry allows us to explicitly see.

Throughout the derivations in sections 3–6, λ serves multiple roles as (1) a regression coefficient linking volumetric changes at the surface and integrated column storage (equation (2)), (2) as an e-folding length scale for exponential covariance fall-off of the subsurface soil moisture profile (equation (10)), and (3) as a variance budget ratio between surface shocks and state variable response (equation (28)). The link between these simultaneous interpretations is both physical—through conservation of water mass—and statistical—through the correlated nature of surface and subsurface dynamics.

The ways in which λ is both a statistical and physical descriptor yield some counter-intuitive applications. Our variance budget accounting implies that using λ as the thickness of a surface layer for a simple bucket model will lead to smaller conservation of mass errors than using the nominal 50-mm sensing depth (even though SMAP likely sees something closer to 50 mm than λ). This is confirmed in previous physical modeling studies (Akbar et al., 2018b, 2019). This may be significant for many terrestrial ecological applications, for example, rooting depth and vegetation/climate feedbacks (Gentine et al., 2012), vegetative reservoir extents in global climate models (Koster & Suarez, 2001; Milly & Dunne, 1994), and irrigation estimation (Lawston et al., 2017).

Estimation of $\widehat{\lambda}$ from daily surface soil moisture and precipitation is hindered by estimates of the regression error (unknowable without profile data) and estimates of evaporative/drainage losses (estimable, but not observed). In situ data shows that the covariances between precipitation and losses are not always what we would expect (Figure 3b), which adds uncertainty to our loss estimates and downstream $\widehat{\lambda}$ estimates (Figure 5b). This could perhaps be overcome by calibrating $\widehat{\lambda}$ estimates to either gravimetric or in situ data (or even land surface model runs), which would then allow back calculation of the loss function variability. Alternatively, loss function estimation could be improved by incorporation of evapotranspiration data, or even a potential evaporation proxy. Fortunately, relative estimation errors diminish with thickness of the surface layer, and so we do not expect changes in biases with soil moisture state.

Comparisons of λ estimates between point-scales and remotely sensed scales (see Figure A2c) suggest that the best estimate of λ is made at the scale of the application. This is, as previously mentioned, due to both representativeness and the dampening of variances with aggregation scale. An additional consideration is that the validity of a simple linear model may change with scale, effectively changing the magnitude of $\sigma^2_{\varepsilon_{reg}}$. This cannot be easily assessed without full profile data at multiple spatial scales, which could perhaps be an avenue of future study within a multiscale physical modeling environment.

8. Conclusions

In this study, we define the *subsurface coupling length* λ as (1) a statistical mean-state estimator for changes in total column water given changes in observed surface soil moisture, (2) the *e*-folding length scale for an exponential covariance profile in the soil column, and (3) the appropriate length scale for a bucket model of the surface to conserve water mass using a variance budget. We provide a formula for estimating λ (equation (28)) using surface soil moisture and precipitation observations (either in situ or remotely sensed).

We show that the surface and subsurface are generally coupled globally, and that λ is typically larger than SMAP's radiometric sensing depth (sometimes by an order of magnitude), implying that satellite soil moisture observations tell us about more of the soil profile than we can explicitly see. That said, since we also find that λ increases with the thickness of the observed surface layer (Figure 2), lower-frequency microwave radiometric instruments will still provide additional benefit in probing the subsurface.

As a step in this process, we derive a method to estimate the lag-one autocorrelation for irregularly observed data (equation (26)) and provide what is, to our knowledge, the first global map of the AR(1) coefficient for surface soil moisture.

We conclude that, in all but the most arid areas, the surface actually tells us more about the total column water than a 50-mm sensing depth would imply. This finding may allow users of microwave soil moisture products to recognize where extrapolation to ecosystem-scale wetting and drying conditions is reasonable and where it is not. The mixed statistical/physical nature of λ allows us to explicitly discuss correlated moisture fluxes in the subsurface, even in situations when physical models cannot be properly parameterized due to lack of data or difficulty in representation of scale.

The subsurface coupling scale may be useful as a predictor of rooting depth (Rama, 1988; Schymanski et al., 2008), which is determined not so much by maximum water extraction (except in arid climates), but by supply consistency. Beyond this, there is some evidence that spatial patterns of λ may moderate soil moisture/evapotranspiration and soil moisture/drainage fluxes (Akbar et al., 2019), which would allow us to translate (unitless) volumetric changes into extrinsic fluxes.

The existence of subsurface coupling makes the unobserved profiles of soil moisture scientifically "visible" from existing surface observations. This additional soil water information allows for more complete representation of drought, land-atmosphere feedbacks, groundwater transfers, moisture availability for vegetated ecosystems, and the coupling of the terrestrial water, energy, and carbon cycles.

Appendix A: Exponential Covariance and Correlation Profiles

Equation (10) from the main text gives an exponential relation for the soil moisture covariance function in depth

$$\exp\left(-\frac{z}{\kappa}\right) = \frac{\theta_s', \theta_z'}{\sigma^2_{\theta_s'}} = \gamma(z).$$

We can plot the actual measured covariances (scaled by the surface variance) versus depth for each of the Airborne Microwave Observatory of Subcanopy and Subsurface (AirMOSS) sites to see whether they fall off exponentially and to determine the *e*-folding scale κ. These relationships are shown in Figure A1a, with red lines showing least-squares best exponential fits. The κ values from those fits are plotted against λ values (from equation (2) directly), using the 2-cm sensors as θ_s as well.

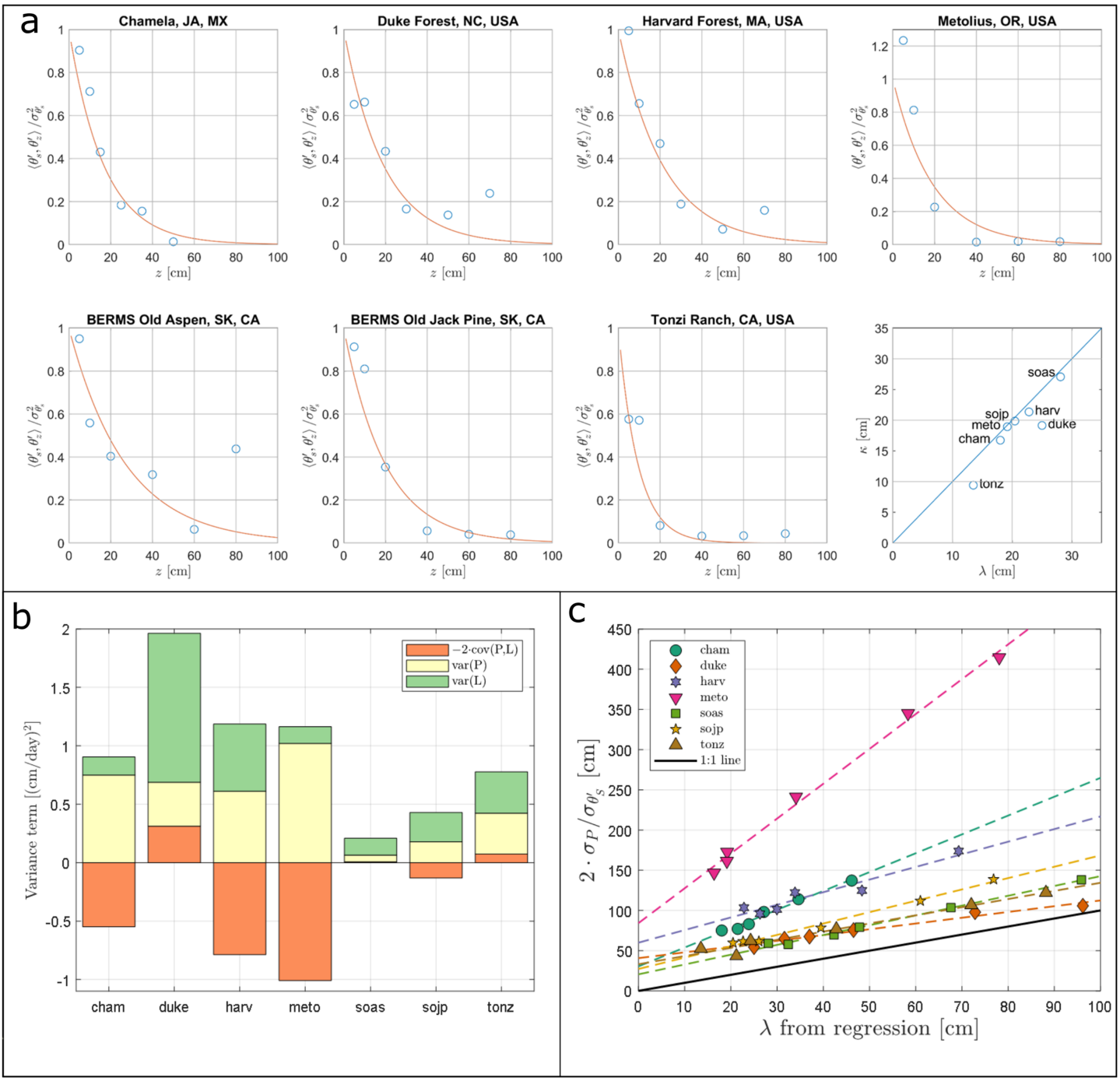

Figure A1. Subsurface/surface variance relations, $\dot{V}$ variance partitioning, and upper bounds at seven in situ sites. (a) Blue circles show covariance between the surface layer and subsurface layers (scaled by surface variance), which generally falls off with increasing depth. Red lines show an exponential fit; scatter plot shows exponential fall-off length scale versus λ from regression at each site clustered near a 1-to-1 line. (b) Partitioning of full-profile $\dot{V}$ term as in equation (A9); precipitation variance does not always dominate, and precipitation/losses sometimes negatively covary. (c) An upper bound λ_{UB} as defined in equation (A11) versus λ directly from regression as a function of surface layer thickness h_1 (h_1 increases to the right in all cases). λ_{UB} is always greater than λ and often much greater.

While the equivalence is quite close for most of the sites, for all sites, $\kappa < \lambda$ (faster than exponential fall-off of covariance), and proximity to the 1-to-1 line shows the degree to which the covariance between the surface and subsurface falls off exponentially. Larger κ (or λ) values mean that the covariance decreases more slowly through the column, that is, the BERMS Old Aspen site has a shallow drop-off in covariance with the surface, while Tonzi Ranch has a steep (and not quite exponential) drop-off in covariance with the surface.

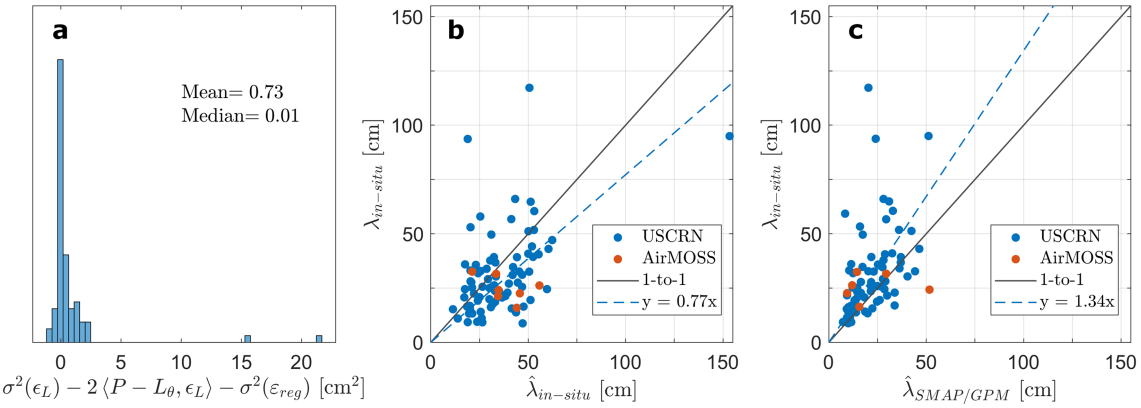

Figure A2. Estimation of $\widehat{\lambda}$ at in situ sites using in situ (surface layer =7.5 cm) and remotely sensed data. (a) Histogram of the unestimatable terms from the numerator in equation (A14), with mean and median near zero (despite outliers). (b) λ as estimated from regression (equation (3)) versus $\widehat{\lambda}$ as estimated from equation (34) at United State Climate Reference Network (USCRN) and AirMOSS in situ sites. Errors are the results only of neglecting the terms shown in (a). (c) $\widehat{\lambda}$ as estimated from regression using in situ measurements versus $\widehat{\lambda}$ as estimated from equation (19) using remotely sensed estimates (Soil Moisture Active Passive [SMAP] soil moisture and Global Precipitation Measurement [GPM] precipitation). Bias and errors are the result of both neglected terms from Figure 5a and spatial representativeness differences—notably the reduction of hydrometeorological variance (P and θ) with aggregation scale.

A1 .Correlation Length Scale

If, instead of assuming an exponential *covariance* profile, we assume exponential *correlation* profiles,

$$\rho\left(\theta_s', \theta_z'\right) = \exp\left(-\frac{z}{\alpha}\right), \tag{A1}$$

but make no assumptions about the variance of soil moisture with depth, then the subsurface coupling length scale can be estimated as a function of the correlation length scale, α, as

$$\lambda = \int_0^{h_1+h_2} \frac{\sigma_{\theta_z'}}{\sigma_{\theta_s'}} \cdot \exp\left(-\frac{z}{\alpha}\right) \mathrm{d}z. \tag{A2}$$

This approximation is shown as red x-es in Figure 2 for each in situ site and is generally more accurate than the exponential covariance profile assumption in equation (10) (the covariance assumption is more restrictive as it constrains the variability at all depths as well as the temporal correlations). If you build on this assumption to assume that the standard deviations of changes in soil moisture fall off exponentially in the soil column,

$$\sigma_{\theta_z'} = \sigma_{\theta_s'} \cdot \exp\left(-\frac{z}{\beta}\right), \tag{A3}$$

then

$$\lambda = \int_0^{h_1+h_2} \exp\left(-\frac{z}{\alpha}\right) \cdot \exp\left(-\frac{z}{\beta}\right) \mathrm{d}z \tag{A4}$$

$$= \left(\frac{1}{\alpha} + \frac{1}{\beta}\right)^{-1} \tag{A5}$$

for large values of h_2. This hyperbolic mean relation implies that, with exponential correlation and standard deviation length scales α and β, respectively, the subsurface coupling length scale is

$$\lambda \approx \min(\alpha, \beta). \tag{A6}$$

Assuming exponential variances rather than standard deviations rescales β by a factor of two. Without resorting to direct empiricism (i.e., regression with site characteristics, soil texture, and meteorology), determination of any of the covariance, correlation, or standard deviation length scales still requires measurements of the subsurface.

A2. Theoretical Bounds on λ

Returning to equation (3c),

$$\lambda = \sqrt{\frac{\sigma^2_{V'} - \sigma^2_{\varepsilon_{reg}}}{\sigma^2_{\theta'_s}}},$$

we notice that the error term decreases the value of λ, such that an upper bound can be defined as

$$\lambda \leq \frac{\sigma_{V'}}{\sigma_{\theta'_s}}. \tag{A7}$$

For perfect coupling between the surface and subsurface (a rigid, constant-shape soil moisture profile), the error term and its standard deviation go to zero and $\lambda \to \sigma_{V'}/\sigma_{\theta'_s}$. For complete decorrelation between the surface and subsurface, we have already seen that $\lambda \to h_1$, the thickness of the observed surface layer, so $h_1 \leq \lambda \leq \sigma_{V'}/\sigma_{\theta'_s}$ (negative daily-scale correlations between the surface and subsurface, giving rise to $\lambda < h_1$ or even $\lambda < 0$, do not occur at any of roughly 100 in situ sites we have available for this study).

The upper bound on λ in equation (A7) depends on the standard deviation of V',

$$\sigma_{V'} = \sqrt{\sigma^2_{\{P-L\}}} \tag{A8}$$

$$= \sqrt{\sigma^2_P + \sigma^2_L - 2P, L}. \tag{A9}$$

The last term in A9—the covariance between P and L—as determined from full profile measurements at the AirMOSS sites, is nonnegligible, quite variable, often of the same order of magnitude as the individual variance terms, and can be positive or negative (daily precipitation is observed and total column losses are calculated daily from the water balance equation (17)). Figure A1b shows a variance budget for the terms in equation (A9). The sum of the magnitudes of the three colored bars gives the variance of changes in total column water for each site, $\sigma^2_{V'}$. Beyond the substantial range of values for the covariance term, it may be surprising to see the relative magnitudes of the loss and precipitation terms, with σ^2_L roughly equal to σ^2_P at Tonzi Ranch, and $\sigma^2_L > \sigma^2_P$ at the Old Aspen and Duke sites by factors of 2.5 and 3.4, respectively. This may be due to variability in drivers of evapotranspiration (discussed below), measurement error, the neglected effects of horizontal advection, or real subsurface process variability. Even as hydrologists, we may sometimes forget that the soil is more than just a phase-shifted low-pass filter on precipitation; it is also, of course, its own complex dynamic system with flows and sinks, actively controlled root systems, diurnal cycles, and nonnegligible capillary rise. Some of these complexities may be reduced by the averaging which necessarily occurs at the remotely sensed pixel scale.

Figure A1b shows that none of the terms in equation (A9) can be ignored—particularly for those sites which are far from the 1-to-1 line in Figure A1a (Tonzi, Duke, Old Aspen)—but we can still write

$$\sigma_{V'} \leq \sqrt{\sigma^2_P + \sigma^2_L + 2\sigma_P\sigma_L} \leq \sqrt{4 \cdot \max(\sigma^2_P, \sigma^2_L)} = 2 \cdot \max(\sigma_P, \sigma_L), \tag{A10}$$

where the first inequality comes from assuming a bounding case with perfect correlation between P and L. While we can see that there are situations in which σ_L is the dominant term, so long as σ_P is of roughly the same order(For a correlation ρ_{PL} between precipitation and losses, $\sigma_{V'} < 2\sigma_P$ if

$$\frac{\sigma_P}{\sigma_L} > \frac{\rho_{PL} + \sqrt{\rho_{PL}^2 + 12}}{6}$$

which ranges between 0.43 and 0.77 with ρ_{PL}.) as σ_L, we can establish an upper bound using the (observable) σ_P as

$$\lambda_{\mathrm{UB}} = 2\frac{\sigma_{\mathrm{P}}}{\sigma_{\theta_s'}}. \tag{A11}$$

Figure A1c shows that this is always true at these sites and that this is not always a tight constraint (for example when both σ_P and $\langle P,L \rangle$ are large, as at Metolius). For each site, the markers show λ_{UB} using different values of h_1, the surface layer thickness (as in Figure 2) with larger λ values again corresponding to larger h_1 values. This simply shows the attenuation of surface layer variance with averaging to depth serving to decrease the denominator in equation (A11). Because of its limited utility as a constraint for these in situ sites, we do not explore λ_{UB} further in this study but do show global estimates in Figure S9.

A3. Loss Function Validation

To estimate λ when in situ observations of subsurface losses are not available, we write our estimated loss function from equation (21) as

$$\mathrm{L}_\theta = \mathrm{E}\{\mathrm{P}|\theta_s\} \tag{A12}$$

and then write its relationship with the true losses in the soil column, L, as

$$\mathrm{L}(t) = \mathrm{L}_\theta(t) + \epsilon_{\mathrm{L}}(t). \tag{A13}$$

L_θ captures variability in losses due to surface soil moisture state, and thus represents the variability in L, which is encoded directly in time series of surface soil moisture and precipitation. The (mean-zero) errors, ϵ_L, are due to variability in other processes, namely deep column moisture state and atmospheric drivers of evaporative losses from the soil column. Deseasoning each of the soil moisture, precipitation, and (estimated) loss time series can reduce components of ϵ_L due to seasonal dynamics (e.g., in vapor pressure deficit, vegetation green-up, and evapotranspiration). To see the effects of estimating separate loss functions by season, see Figures S4, S5, and S7.

Using the conditionally averaged loss estimates, we can rewrite equation (3c) as follows:

$$\begin{aligned}\lambda &= \sqrt{\frac{\sigma_{\mathrm{V}'}^2 - \sigma_{\epsilon_{\mathrm{reg}}}^2}{\sigma_{\theta_s'}^2}} \\ &= \sqrt{\frac{\sigma_{\mathrm{P-L}_\theta-\epsilon_{\mathrm{L}}}^2 - \sigma_{\epsilon_{\mathrm{reg}}}^2}{\sigma_{\theta_s'}^2}} \\ &= \sqrt{\frac{\sigma_{\mathrm{P}}^2 + \sigma_{\mathrm{L}_\theta}^2 - 2\mathrm{P},\mathrm{L}_\theta + \sigma_{\epsilon_{\mathrm{L}}}^2 - 2\mathrm{P}-\mathrm{L}_\theta,\epsilon_{\mathrm{L}} - \sigma_{\epsilon_{\mathrm{reg}}}^2}{\sigma_{\theta_s'}^2}}.\end{aligned} \tag{A14}$$

In the numerator, we can calculate the first three terms $\sigma_P^2, \sigma_{L_\theta}^2$, and $\langle P, L_\theta \rangle$ from time series of P and θ_s alone. The remaining three terms, $\sigma_{\epsilon_L}^2$, $\langle P - L_\theta, \epsilon_L \rangle$, and $\sigma_{\epsilon_{reg}}^2$ require the full integrated profile time series of V, rendering them unestimable from satellite surface soil moisture and precipitation.

To assess the impact of neglecting the contributions of the three unestimatable terms, we can calculate them at in situ sites with full profile V time series. Figure A2a shows a histogram of the three terms at 81 sites from the USCRN. Despite the fact that both ϵ_L and ϵ_{reg} are on the same order as σ_P^2, the sum of the three is typically near zero (Figure 5a). This leads us to define

$$\widehat{\lambda} \equiv \frac{\sigma_{P-L_\theta}}{\sigma_{\theta_s'}} \tag{A15}$$

as a tractable estimator of λ.

This estimate will depend on the observed surface layer depth (as demonstrated in Figure 2), as well as on the spatial scale of aggregation of the input variables, P and θ (temporal variances decrease with increased spatial aggregation). Although we cannot directly validate this approximation at the scale of remotely sensed P and θ observations, we can with the in situ data, as shown in Figure A2b. Neglecting the unestimatable terms does introduce some significant bias suggesting that $\widehat{\lambda}$ estimates from equation (A15) may (on average) slightly overestimate the "true" subsurface coupling length (by ~29%). It is worth noting here that even the "true" estimates of λ from regression are of course least-squares estimations and subject to sampling variability themselves.

Fortunately, the biases appear to diminish with increasing surface layer thickness h_1, at least in a relative sense. The mean $\sqrt{\sigma^2_{\epsilon_L} - 2P - L_\theta, \epsilon_L - \sigma^2_{\epsilon_{reg}}}$ when $h_1 = 125$ cm is only 1.1336 cm at the USCRN sites, roughly twice as large as when $h_1 = 7.5$ cm, while λ increases much more rapidly (see Figure 2a). This implies that errors in λ estimation should not increase simply due to dry soil conditions (which serve to increase the radiometric emission depth, h_1 for satellite retrievals). Additionally, lower frequency sensors would be subject to smaller relative estimation errors.

A4. In Situ versus Satellite Intercomparison

Values of λ from the USCRN and AirMOSS in situ sites are shown versus estimates of $\widehat{\lambda}$ from SMAP and GPM in Figure A2c. Significantly, the observational time periods do *not* overlap between the SMAP/GPM record and the AirMOSS observations, while they do for SMAP/GPM and the USCRN data. For the in situ observations, the surface soil layer is defined as the top 7.5 cm. $\widehat{\lambda}$ from remotely sensed observations is on average lower than the in situ regression λ in Figure A2c. This is opposite of the response in Figure A2b, and we would assume that spatial scaling and representativeness play a large role in determining the subsurface coupling scale length (i.e., that the variance of fluxes decreases more rapidly with increasing spatial scale than does the variance of the changes in volumetric soil moisture—a bounded variable). From the perspective of equation (28), this makes sense; the variance terms decrease and the lag-one autocorrelation increases when aggregated to the pixel-scale, but it is not clear that they would scale similarly. At a more conceptual level, both the statistical and physical coupling between the surface and the subsurface may behave quite differently for a point-scale measurement versus for a 9 km × 9 km landscape; we would not necessarily expect a 1-to-1 equivalence between the in situ and remotely sensed length scales. While λ does represent a physical correlation scale, we expect it to have scale dependence, and so a particular length scale may be primarily representative of a particular data set or spatial extent.

Acknowledgments
AcknowledgementsThe authors acknowledge funding from NASA in the form of a sponsored research grant. Soil moisture data from SMAP are available for download from the National Snow Ice Data Center (NSIDC) Distributed Active Archive Center (DAAC) at https://nsidc.org/data/smap/smap-data.html. Precipitation data from GPM is available at https://pmm.nasa.gov/data-access/downloads/gpm.

References

Akbar, R., Short Gianotti, D., McColl, K. A., Haghighi, E., Salvucci, G. D., & Entekhabi, D. (2018b). Hydrological storage length scales represented by remote sensing estimates of soil moisture and precipitation. *Water Resources Research*, 1476–1492. https://doi.org/10.1002/2017WR021508

Akbar, R., Short Gianotti, D. J., Salvucci, G. D., & Entekhabi, D. (2019). Mapped hydroclimatology of evapotranspiration and drainage runoff using SMAP brightness temperature observations and precipitation information. *Water Resources Research*, *55*, 3391–3413.

Akbar, R., Short Gianotti, D. J., McColl, K. A., Haghighi, E., Salvucci, G. D., & Entekhabi, D. (2018a). Hydrological storage length scales represented by remote sensing estimates of soil moisture and precipitation. *Water Resources Research*, *54*, 1476–1492. https://doi.org/10.1002/2017WR021508

Albergel, C., Rüdiger, C., Pellarin, T., Calvet, J.-C., Fritz, N., Froissard, F., et al. (2008). From near-surface to root-zone soil moisture using an exponential filter: An assessment of the method based on in-situ observations and model simulations. *Hydrology and Earth System Sciences Discussions*, *5*(3), 1603–1640. https://doi.org/10.5194/hessd-5-1603-2008

Albergel, C., Dutra, E., Bonan, B., Zheng, Y., Munier, S., Balsamo, G., et al. (2019). Monitoring and forecasting the impact of the 2018 summer heatwave on vegetation. *Remote Sensing*, *11*(5). https://doi.org/10.3390/rs11050520

Barichivich, J., Briffa, K. R., Myneni, R., van der Schrier, G., Dorigo, W., Tucker, C. J., et al. (2014). Temperature and snow-mediated moisture controls of summer photosynthetic activity in northern terrestrial ecosystems between 1982 and 2011. *Remote Sensing*, *6*(2), 1390–1431. https://doi.org/10.3390/rs6021390

Bartalis, Z., Wagner, W., Naeimi, V., Hasenauer, S., Scipal, K., Bonekamp, H., et al. (2007). Initial soil moisture retrievals from the METOP-A Advanced Scatterometer (ASCAT). *Geophysical Research Letters*, *34*, L20401. https://doi.org/10.1029/2007GL031088

Bell, J. E., Palecki, M. A., Baker, C. B., Collins, W. G., Lawrimore, J. H., Leeper, R. D., et al. (2013). U.S. climate reference network soil moisture and temperature observations. *Journal of Hydrometeorology*, *14*(3), 977–988. https://doi.org/10.1175/JHM-D-12-0146.1

Bolten, J. D., & Crow, W. T. (2012). Improved prediction of quasi-global vegetation conditions using remotely-sensed surface soil moisture. *Geophysical Research Letters*, *39*, L19406. https://doi.org/10.1029/2012GL053470

Brodzik, M. J., Billingsley, B., Haran, T., Raup, B., & Savoie, M. H. (2012). EASE-Grid 2.0: Incremental but Significant Improvements for Earth-gridded data sets. *ISPRS International Journal of Geo-Information*, *1*(3), 32–45. https://doi.org/10.3390/ijgi1010032

Calvet, J.-C., & Noilhan, J. (2000). From near-surface to root-zone soil moisture using year-round data. *Journal of Hydrometeorology*, *1*(5), 393–411. https://doi.org/10.1175/1525-7541(2000)001 < 0393:FNSTRZ>2.0.CO;2

Ceballos, A., Scipal, K., Wagner, W., & Martínez-Fernández, J. (2005). Validation of ERS scatterometer-derived soil moisture data in the central part of the Duero Basin, Spain. *Hydrological Processes*, *19*(8), 1549–1566. https://doi.org/10.1002/hyp.5585

Ciais, P., Reichstein, M., Viovy, N., Granier, A., Ogée, J., Allard, V., et al. (2005). Europe-wide reduction in primary productivity caused by the heat and drought in 2003. *Nature*, *437*(7058), 529–533. https://doi.org/10.1038/nature03972

Crow, W. T., Han, E., Ryu, D., Hain, C. R., & Anderson, M. C. (2017). Estimating annual water storage variations in medium-scale (2000-10000 km2) basins using microwave-based soil moisture retrievals. *Hydrology and Earth System Sciences*, *21*(3), 1849–1862. https://doi.org/10.5194/hess-21-1849-2017

Cuenca, R. H., Hagimoto, Y., Ring, T. M., & Beamer, J. P. (2016). Interpretation of in situ observations in support of P-band radar retrievals. *IEEE Journal of Selected Topics in Applied Earth Observations and Remote Sensing*, *9*(7), 3122–3130. https://doi.org/10.1109/JSTARS.2016.2582737

Entekhabi, D., Nakamura, H., & Njoku, E. G. (1994). Solving the inverse problem for soil moisture and temperature\nprofiles by sequential assimilation of multifrequency remotely sensed\nobservations. *IEEE Transactions on Geoscience and Remote Sensing*, *32*(2), 438–448. https://doi.org/10.1109/36.295058

Entekhabi, D., Njoku, E. G., O'Neill, P. E., Kellogg, K. H., Crow, W. T., Edelstein, W. N., et al. (2010). The Soil Moisture Active Passive (SMAP) mission. *Proceedings of the IEEE*, *98*(5), 704–716. https://doi.org/10.1109/JPROC.2010.2043918

Entekhabi, D., Yueh, S., O'Neil, P. E., Kellogg, K. H., Allen, A., & Bindlish, R. (2014). *SMAP Handbook* (No. JPL 400-1567). Pasadena, CA: National Aeronautics and Space Administration.

Escorihuela, M. J., Chanzy, A., Wigneron, J. P., & Kerr, Y. H. (2010). Effective soil moisture sampling depth of L-band radiometry: A case study. *Remote Sensing of Environment*, *114*(5), 995–1001. https://doi.org/10.1016/j.rse.2009.12.011

Ford, T. W., Harris, E., & Quiring, S. M. (2014). Estimating root zone soil moisture using near-surface observations from SMOS. *Hydrology and Earth System Sciences*, *18*(1), 139–154. https://doi.org/10.5194/hess-18-139-2014

Gentine, P., D'Odorico, P., Lintner, B. R., Sivandran, G., & Salvucci, G. (2012). Interdependence of climate, soil, and vegetation as constrained by the Budyko curve. *Geophysical Research Letters*, *39*, L19404. https://doi.org/10.1029/2012GL053492

Green, J. K., Seneviratne, S. I., Berg, A. M., Findell, K. L., Lawrence, D. M., & Gentine, P. (2019). Large influence of soil moisture variability on long-term terrestrial carbon uptake. *Nature*, *565*(7740), 476–479. https://doi.org/10.1038/s41586-018-0848-x

Haghighi, E., Short Gianotti, D. J., Akbar, R., Salvucci, G. D., & Entekhabi, D. (2018). Soil and atmospheric controls on the land surface energy balance: A generalized framework for distinguishing moisture-limited and energy-limited evaporation regimes. *Water Resources Research*, 1831–1851. https://doi.org/10.1002/2017WR021729

Hirschi, M., Seneviratne, S. I., Alexandrov, V., Boberg, F., Boroneant, C., Christensen, O. B., et al. (2011). Observational evidence for soil-moisture impact on hot extremes in southeastern Europe. *Nature Geoscience*, *4*(1), 17–21. https://doi.org/10.1038/ngeo1032

Hou, A. Y., Kakar, R. K., Neeck, S., Azarbarzin, A. A., Kummerow, C. D., Kojima, M., et al. (2014). The global precipitation measurement mission. *Bulletin of the American Meteorological Society*, *95*(5), 701–722. https://doi.org/10.1175/BAMS-D-13-00164.1

Houser, P. R., Shuttleworth, W. J., Famiglietti, J. S., Gupta, H. V., Syed, K. H., & Goodrich, D. C. (1998). Integration of soil moisture remote sensing and hydrologic modeling using data assimilation. *Water Resources Research*, *34*(12), 3405–3420. https://doi.org/10.1029/1998WR900001

Huffman, G. J., Bolvin, D. T., & Nelkin, E. J. (2017). Integrated Multi-satellitE Retrievals for GPM (IMERG), V04A. Retrieved March 25, 2017, from https://pmm.nasa.gov/

Imaoka, K., Maeda, T., Kachi, M., Kasahara, M., Ito, N., & Nakagawa, K. (2012). Status of AMSR2 instrument on GCOM-W1, *852815* (November 2012), 852815. https://doi.org/10.1117/12.977774

Jung, M., Reichstein, M., Ciais, P., Seneviratne, S. I., Sheffield, J., Goulden, M. L., et al. (2010). Recent decline in the global land evapotranspiration trend due to limited moisture supply. *Nature*, *467*(7318), 951–954. https://doi.org/10.1038/nature09396

Kawanishi, T., Sezai, T., Ito, Y., Imaoka, K., Takeshima, T., Ishido, Y., et al. (2003). The Advanced Microwave Scanning Radiometer for the Earth Observing System (AMSR-E), NASDA's contribution to the EOS for global energy and water cycle studies. *IEEE Transactions on Geoscience and Remote Sensing*, *41*(2), 184–194. https://doi.org/10.1109/TGRS.2002.808331

Kerr, Y. H., Waldteufel, P., Wigneron, J.-P., Delwart, S., Cabot, F., Boutin, J., et al. (2010). The SMOS mission: New tool for monitoring key elements of the global water cycle. *Proceedings of the IEEE*, *98*(5), 666–687. https://doi.org/10.1109/JPROC.2010.2043032

Kerr, Y. H., Waldteufel, P., Wigneron, J. P., Martinuzzi, J. M., Font, J., & Berger, M. (2001). Soil moisture retrieval from space: The Soil Moisture and Ocean Salinity (SMOS) mission. *IEEE Transactions on Geoscience and Remote Sensing*, *39*(8), 1729–1735. https://doi.org/10.1109/36.942551

Kirchner, J. W. (2009). Catchments as simple dynamical systems: Catchment characterization, rainfall-runoff modeling, and doing hydrology backward. *Water Resources Research*, *45*, W02429. https://doi.org/10.1029/2008WR006912

Koster, R. D., Dirmeyer, P. A., Guo, Z., Bonan, G., Chan, E., Cox, P., et al., & GLACE Team (2004). Regions of strong coupling between soil moisture and precipitation. *Science*, *305*(5687), 1138–1140. https://doi.org/10.1126/science.1100217

Koster, R. D., & Suarez, M. J. (2001). Soil moisture memory in climate models. *Journal of Hydrometeorology*, *2*(6), 558–570. https://doi.org/10.1175/1525-7541(2001)002 < 0558:SMMICM>2.0.CO;2

Kumar, S. V., Jasinski, M., Mocko, D., Rodell, M., Borak, J., Li, B., et al. (2019). NCA-LDAS land analysis: Development and performance of a multisensor, multivariate land data assimilation system for the National Climate Assessment. *Journal of Hydrometeorology*, *20*(8), 1571–1593. https://doi.org/10.1175/JHM-D-17-0125.1

Kumar, S. V., Reichle, R. H., Koster, R. D., Crow, W. T., & Peters-Lidard, C. D. (2009). Role of subsurface physics in the assimilation of surface soil moisture observations. *Journal of Hydrometeorology*, *10*(6), 1534–1547. https://doi.org/10.1175/2009JHM1134.1

Lawston, P. M., Santanello, J. A., & Kumar, S. V. (2017). Irrigation signals detected from SMAP soil moisture retrievals. *Geophysical Research Letters*, *44*, 11,860–11,867. https://doi.org/10.1002/2017GL075733

Legates, D. R., Mahmood, R., Levia, D. F., DeLiberty, T. L., Quiring, S. M., Houser, C., & Nelson, F. E. (2011). Soil moisture: A central and unifying theme in physical geography. *Progress in Physical Geography*, *35*(1), 65–86. https://doi.org/10.1177/0309133310386514

Li, J., & Islam, S. (1999). On the estimation of soil moisture profile and surface fluxes partitioning from sequential assimilation of surface layer soil moisture. *Journal of Hydrology*, *220*(1–2), 86–103. https://doi.org/10.1016/S0022-1694(99)00066-9

McColl, K. A., Alemohammad, S. H., Akbar, R., Konings, A. G., Yueh, S., & Entekhabi, D. (2017). The global distribution and dynamics of surface soil moisture. *Nature Geoscience*, *10*(2), 100–104. https://doi.org/10.1038/ngeo2868

Milly, P. C. D. (1993). An analytic solution of the stochastic storage problem applicable to soil water. *Water Resources Research*, *29*(11), 3755–3758. https://doi.org/10.1029/93WR01934

Milly, P. C. D. (1997). Sensitivity of greenhouse summer dryness to changes in plant rooting characteristics. *Geophysical Research Letters*, *24*(3), 269–271.

Milly, P. C. D., & Dunne, K. A. (1994). Sensitivity of the global water cycle to the water-holding capacity of land. *Journal of Climate*, *7*(4), 506–526. https://doi.org/10.1175/1520-0442(1994)007 < 0506:SOTGWC>2.0.CO;2

Miralles, D. G., Teuling, A. J., Van Heerwaarden, C. C., & De Arellano, J. V. G. (2014). Mega-heatwave temperatures due to combined soil desiccation and atmospheric heat accumulation. *Nature Geoscience*, *7*(5), 345–349. https://doi.org/10.1038/ngeo2141

Mu, Q., Zhao, M., & Steven W. Running. (2013). Algorithm theoretical basis document: MODIS global terrestrial evapotranspiration (ET) product (NASA MOD16A2/A3). National Aeronautics and Space Administration.

Mueller, B., & Seneviratne, S. I. (2012). Hot days induced by precipitation deficits at the global scale. *Proceedings of the National Academy of Sciences*, *109*(31), 12398–12403. https://doi.org/10.1073/pnas.1204330109

Muñoz, A. A., Barichivich, J., Christie, D. A., Dorigo, W., Sauchyn, D., González-Reyes, Á., et al. (2014). Patterns and drivers of Araucaria araucana forest growth along a biophysical gradient in the northern Patagonian Andes: Linking tree rings with satellite observations of soil moisture. *Austral Ecology*, *39*(2), 158–169. https://doi.org/10.1111/aec.12054

Musyimi, Z. (2011). Temporal Relationships Between Remotely Sensed Soil Moisture and NDVI Over Africa: Potential for Drought Early Warning? University of Twenty.

Njoku, E. G., & Entekhabi, D. (1996). Passive microwave remote sensing of soil moisture. *Journal of Hydrology*, *184*(1–2), 101–129. https://doi.org/10.1016/0022-1694(95)02970-2

O'Neill, P. E., Chan, S., Njoku, E. G., Jackson, T., & Bindlish, R. (2016). *SMAP enhanced L3 radiometer global daily 9 km EASE-grid soil moisture, version 1*. Boulder, Colorado USA: NASA National Snow and Ice Data Center Distributed Active Archive Center. https://doi.org/doi https://doi.org/10.5067/ZRO7EXJ8O3XI

Qiu, J., Crow, W. T., & Nearing, G. S. (2016). The impact of vertical measurement depth on the information content of soil moisture for latent heat flux estimation. *Journal of Hydrometeorology*, *17*, 2419–2430. https://doi.org/10.1175/JHM-D-16-0044.1

Qiu, J., Crow, W. T., Nearing, G. S., Mo, X., & Liu, S. (2014). The impact of vertical measurement depth on the information content of soil moisture times series data. *Geophysical Research Letters*, *41*, 4997–5004. https://doi.org/10.1175/JHM-D-16-0044.1

Ragab, R. (1995). Towards a continuous operational system to estimate the root-zone soil moisture from intermittent remotely sensed surface moisture. *Journal of Hydrology*, *173*(1–4), 1–25. https://doi.org/10.1016/0022-1694(95)02749-F

Raju, S., Chanzy, A., Wigneron, J.-P., Calvet, J.-C., Kerr, Y., & Laguerre, L. (1995). Soil moisture and temperature profile effects on microwave emission at low frequencies. *Remote Sensing of Environment*, *54*(2), 85–97. https://doi.org/10.1016/0034-4257(95)00133-L

Rama, P. (1988). A linear root water uptake model. *Journal of Hydrology*, *99*, 297–306. https://doi.org/10.1016/0022-1694(88)90055-8

Reichle, R. H., Crow, W. T., & Keppenne, C. L. (2008). An adaptive ensemble Kalman filter for soil moisture data assimilation. *Water Resources Research*, *44*, W03423. https://doi.org/10.1029/2007WR006357

Reichle, R. H., De Lannoy, G. J. M., Liu, Q., Ardizzone, J. V., Colliander, A., Conaty, A., et al. (2017). Assessment of the SMAP Level-4 surface and root-zone soil moisture product using in situ measurements. *Journal of Hydrometeorology*, *18*(10), 2621–2645. https://doi.org/10.1175/JHM-D-17-0063.1

Reichle, R. H., Koster, R. D., Liu, P., Mahanama, S. P. P., Njoku, E. G., & Owe, M. (2007). Comparison and assimilation of global soil moisture retrievals from the Advanced Microwave Scanning Radiometer for the Earth Observing System (AMSR-E) and the Scanning Multichannel Microwave Radiometer (SMMR). *Journal of Geophysical Research-Atmospheres*, *112*(9), 1–14. https://doi.org/10.1029/2006JD008033

Rigden, A. J., Salvucci, G. D., Entekhabi, D., & Short Gianotti, D. J. (2018). Partitioning evapotranspiration over the continental United States using weather station data. *Geophysical Research Letters*, *45*(18), 9605–9613. https://doi.org/10.1029/2018GL079121

Sabater, J. M., Jarlan, L., Calvet, J.-C., Bouyssel, F., & De Rosnay, P. (2007). From near-surface to root-zone soil moisture using different assimilation techniques. *Journal of Hydrometeorology*, *8*(2), 194–206. https://doi.org/10.1175/JHM571.1

Salvucci, G. D. (2001). Estimating the moisture dependence of root zone water loss using conditionally averaged precipitation. *Water Resources Research*, *37*(5), 1357–1365.

Salvucci, G. D., & Entekhabi, D. (2011). An alternate and robust approach to calibration for the estimation of land surface model parameters based on remotely sensed observations. *Geophysical Research Letters*, *38*, L16404. https://doi.org/10.1029/2011GL048366

Schymanski, S. J., Sivapalan, M., Roderick, M. L., Beringer, J., & Hutley, L. B. (2008). An optimality-based model of the coupled soil moisture and root dynamics. *Hydrology and Earth System Sciences*, *12*, 913–932.

Short Gianotti, D. J., Rigden, A. J., Salvucci, G. D., & Entekhabi, D. (2019). Satellite and station observations demonstrate water availability's effect on continental-scale evaporative and photosynthetic land surface dynamics. *Water Resources Research*, *55*(1), 540–554. https://doi.org/10.1029/2018WR023726

Swenson, S. C. (2012). GRACE monthly land water mass grids NETCDF RELEASE 5.0. PO.DAAC, CA USA.

Tabatabaeenejad, A., Burgin, M., Duan, X., & Moghaddam, M. (2015). P-band radar retrieval of subsurface soil moisture profile as a second-order polynomial: First AirMOSS results. *IEEE Transactions on Geoscience and Remote Sensing*, *53*(2), 645–658. https://doi.org/10.1109/TGRS.2014.2326839

Taylor, C. M., De Jeu, R. A. M., Guichard, F., Harris, P. P., & Dorigo, W. A. (2012). Afternoon rain more likely over drier soils. *Nature*, *489*(7416), 423–426. https://doi.org/10.1038/nature11377

Ulaby, F. T., Moore, R. K., & Fung, A. K. (1986). *Microwave Remote Sensing, Active and Passive, Volume I, Microwave Remote Sensing Fundamentals and Radiometry*. Reading, MA: Addison-Wesley.

Van der Molen, M. K., Dolman, A. J., Ciais, P., Eglin, T., Gobron, N., Law, B. E., et al. (2011). Drought and ecosystem carbon cycling. *Agricultural and Forest Meteorology*, *151*(7), 765–773. https://doi.org/10.1016/j.agrformet.2011.01.018

Wang, J. R., & Schmugge, T. J. (1980). An empirical model for the complex dielectric permittivity of soils as a function of water content. *IEEE Transactions on Geoscience and Remote Sensing*, *GE-18*(4), 288–295.

Zhou, F. C., Song, X., Leng, P., & Li, Z. L. (2016). An effective emission depth model for passive microwave remote sensing. *IEEE Journal of Selected Topics in Applied Earth Observations and Remote Sensing*, *9*(4), 1752–1760. https://doi.org/10.1109/JSTARS.2016.2525801